

21.2% GaAs Solar Cell Using Bilayer Electron Selective Contact

Vidur Raj,* Tuomas Haggren,* Yahuitl Osorio Mayon, Chennupati Jagadish, and Hark Hoe Tan

GaAs remains one of the crucial materials for solar cell applications as it boasts the world's highest efficiency single-junction solar cells. However, their high cost limits their widespread terrestrial applications. Traditional GaAs solar cells require a complex stack of doped junctions, which can only be grown using epitaxy, which is a very costly technique. Herein, a nonepitaxial bilayer of ZnO and TiO₂ as electron-selective contact is studied. It is shown that a bilayer selective contact can achieve very high performance through interface band engineering and a reduction of the barrier for electron transfer. 21.2% efficient solar cells is achieved, with V_{oc} of 1.04 V, J_{sc} of 26.13 mA cm⁻², and a fill factor of 77.8%. The V_{oc} reported in the article is comparable to the highest V_{oc} reported for substrate-based GaAs solar cells of 1.075 V. An experimental loss analysis shows that the device is mainly limited by series and shunt resistance and reflection losses, both of which can further be minimized by optimization of the fabrication process. The results presented will be very useful for the further development of cheaper GaAs solar cells, whereas the bilayer selective contact concept can be implemented for other kinds of solar cells.

1. Introduction

III–V semiconductors such as InP and GaAs remain critical for the continued expansion of photovoltaics for terrestrial applications because they allow for functionalities such as high flexibility, high stability, and high power per unit surface area compared to solar cell materials such as silicon, CZTS, or perovskite.^[1,2] However, their wide-scale implementation is limited by the high cost associated with their fabrication.^[3–5] For example, the cost of III–V solar cells, such as GaAs solar cells, can be more than 100 times that of silicon solar cells.^[3] According to a National Renewable Energy Laboratory cost analysis, metal-organic chemical vapor deposition (MOCVD) growth and maintenance and the requirement for gold-based front and back contact remain two significant drivers of their high cost.^[3] In recent years, there


has been some research on developing techniques to overcome these challenges. For example, new technologies such as hydride vapor phase epitaxy and thin-film vapor–liquid–solid have shown promise in overcoming the cost limitations of MOCVD-based growth, but these techniques cannot achieve material quality as high as MOCVD.^[1,6] Therefore, more research is required to achieve new and innovative device designs in the field of III–V solar cells that circumvent for low quality of absorber material. One such technology is the use of nonepitaxial charge carrier selective contact for charge carrier separation and collection,^[7] and reduced reliance on MOCVD for the growth of highly complex epitaxial structures for performing charge carrier separation and collection.^[8–10]

In recent years, carrier selective contact devices have emerged as an efficient alternative to conventional p–n junction solar cells.^[11,12] The superiority of electron and hole selective contacts over conventional heavily doped p–n regions for charge carrier separation has become apparent in recent years, and today electron and hole selective contacts have become the primary technology to achieve high-efficiency commercial-scale silicon solar cells.^[13] A similar trend can be seen in organic photovoltaics,^[14] perovskites,^[15] chalcogenides,^[5,16] and other thin-film photovoltaics,^[8,17] where the use of carrier selective contacts can lead to efficiency enhancement and overall better performance. The importance of a wide bandgap material with optical transparency and proper band alignment with the

V. Raj
Advanced Research Centre
James Watt School of Engineering
University of Glasgow
Glasgow G11 6EW, UK
E-mail: vidur.raj@glasgow.ac.uk

T. Haggren, C. Jagadish, H. H. Tan
ARC Centre of Excellence for Transformative Meta-Optical Systems
Department of Electronic Materials Engineering
Research School of Physics
The Australian National University
Canberra, ACT 2600, Australia
E-mail: Tuomas.Haggren@anu.edu.au

Y. O. Mayon
School of Engineering
The Australian National University
Canberra, ACT 2600, Australia

 The ORCID identification number(s) for the author(s) of this article can be found under <https://doi.org/10.1002/solr.202300889>.

© 2024 The Authors. Solar RRL published by Wiley-VCH GmbH. This is an open access article under the terms of the Creative Commons Attribution License, which permits use, distribution and reproduction in any medium, provided the original work is properly cited.

DOI: 10.1002/solr.202300889

absorber layer for high-performance of solar cells has been well known for several decades. However, only recently the use of the term “carrier selective contact” has become a norm since the success of “heterojunction with intrinsic thin layer” solar cells.^[12]

Moreover, there has also been a fair amount of study on the beneficial effects of bilayer selective contact, especially for perovskite and organic solar cells.^[18] It has been shown that the interface between the absorber and selective contact can be engineered by using a bilayer to facilitate electron charge separation and collection by reducing the barrier for charge flow, reducing interface defect density, and improving passivation.^[18] These effects are a result of modified interface chemistry and the interface dipole moment.

Unfortunately, research on carrier selective contact for III–V solar cells is rather limited, even though the benefits of carrier selective contact-based III–V solar cells are several-fold, especially from a commercial perspective, as discussed in detail in refs. [1,11]. This is most probably because of the preconceived notion that high-efficiency III–V solar cells can only be achieved using a complex stack of III–V epitaxial thin films. However, this notion has been challenged through a series of theoretical and experimental works, where carrier selective contacts can achieve performance comparable to epitaxial III–V solar cells.^[1,7–11,17,19,20] For example, we recently reported a GaAs solar cell using ZnO as electron selective contact (ESC) to achieve 18.5% efficient solar cell with a V_{oc} of 880 mV.^[19]

In this article, to overcome the limitations of a single-layer selective contact, we employ a bilayer selective contact. We show that by using a bilayer selective contact based on TiO₂ and ZnO, the GaAs solar cell performance can be significantly boosted. We perform a comprehensive study to elucidate the mechanism of the improved performance. Moreover, when an optimized bilayer selective contact is used in combination with a back surface field (BSF) layer grown on 6° off-axis substrate, the

efficiency of the solar cells improves to 21.2%, with a V_{oc} of 1.04 V, which is comparable to the highest reported V_{oc} for substrate-based GaAs solar cell. This work will significantly boost the recent efforts in realizing III–V solar cells using carrier selective contacts.

2. Experimental Section

To study the bilayer selective contact, we fabricated devices on two different kinds of substrates, i.e., on-axis 100 substrates and 6° offcut toward (111 A). From here onward, we denote, the device grown on-axis 100 GaAs substrate as device 1, whereas the device grown on 6° off-axis GaAs substrate as device 2 (see **Figure 1**). Fabrication of both devices 1 and 2 was similar, starting with the epitaxial growth of 1.8 μm *i*-GaAs, followed by the growth of a 15 nm *i*-InGaP passivation epilayer using the Aixtron MOCVD system. The back contact on the wafer with *i*-InGaP/*i*-GaAs epitaxial layers was formed by annealing sputter-coated (AJA 1800) Zn: Au (10:100 nm) thin film at 400 °C in the presence of forming gas. Subsequently, to compare the effect of bilayer selective contact, four different samples were prepared for both device 1 and device 2. Sample 1 contained only ZnO as ESC, sample 2 contained only TiO₂ as ESC, sample 3 contained TiO₂/ZnO bilayer as ESC, and sample 4 contained ZnO/TiO₂ bilayer as ESC. As per convention, ZnO/TiO₂ means ZnO has been deposited on top of TiO₂ and vice versa. Both ZnO and TiO₂ were deposited at 350 °C using RF sputtering system from AJA. Based on initial optimization, for ZnO deposition, a 60 W power was used, whereas for TiO₂ deposition, a power of 130 W was used with an Ar flow rate of 10 sccm and pressure of 1.5 mTorr. Subsequently, an ITO layer was deposited at room temperature using sputtering with the Ar flow rate of 20 sccm and pressure of 1.5 mTorr, at a fixed RF power of 65 W. The total thickness of the oxide layer (i.e., the thickness of ITO + TiO₂ + ZnO) was fixed at about 70 nm to achieve antireflective properties between the wavelength range of 500–600 nm, coinciding with the maximum

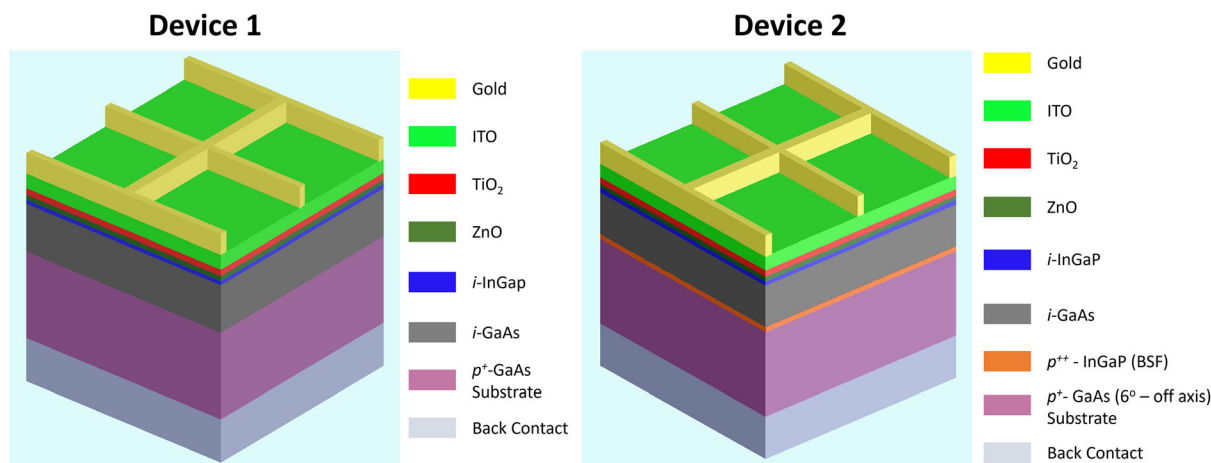


Figure 1. 3D schematic of two different kinds of solar cells that we will discuss in this article (for description, see Experimental Section). For both device 1 and device 2, we study the effect of bilayer selective contact. In a previous report, we already showed ZnO as an ESC ref. [19], and studied different deposition conditions for ZnO as an ESC, with and without *i*-InGaP passivation layer. This article is an extension of the previous study, and instead of ZnO, we use bilayer selective contacts (i.e., ZnO/TiO₂ and TiO₂/ZnO). As per convention, ZnO/TiO₂ means ZnO has been deposited on top of TiO₂ and vice versa.

irradiance of the solar spectrum. Finally, a front contact of Ti/Au (10/100 nm) was deposited on top of ITO using Temescal BJD-2000 e-beam evaporator.

Additionally, previous research on conventional solar cells has shown that a higher V_{oc} can be obtained for solar cells with a BSF and absorber layer grown on off-axis GaAs substrates.^[21–24] The p^{++} BSF layer creates a built-in electric field that reflects electrons at the interface, thereby reducing the recombination, which improves the V_{oc} of the solar cell.^[25] p^{++} BSF layer can also be considered as a hole selective layer, where heavy p -type doping ensures asymmetric conductivity toward holes and assists in the efficient charge carrier separation at the interface.^[26] At the same time, the growth of p^{++} -InGaP BSF layer on the off-axis substrate helps modify its optoelectronic and crystal quality, leading to an overall higher performance of the solar cell.^[21,22] Therefore, after optimization of a bilayer, we use an off-axis substrate with a BSF layer (as shown in Figure 1b) to study the maximum potential of the solar cell, mainly in terms of V_{oc} . We call this solar cell structure device 2. The parameters for deposition of ZnO and TiO₂ were same as device 1.

The passivation characteristics of InGaP before and after ZnO and/or TiO₂ depositions were carried out using a homemade time-resolved photoluminescence setup to ensure that oxide deposition did not deteriorate the surface passivation of the absorber. The dark and light I - V characteristics of the fabricated devices were measured using an Oriel I - V test station and an Oriel quantum efficiency measurement setup. Before each measurement, the I - V test station and the external quantum efficiency (EQE) test setup were calibrated to 1 sun (100 mW cm⁻²) at 25 °C using a silicon reference solar cell. However, we acknowledge that there is a spectral mismatch between the reference cell and the test cell, and we could not correct for it. Nonetheless, to make sure that we do not overestimate J_{sc} of our solar cell, we corroborate our J_{sc} measured using I - V measurement with J_{sc} calculated using the data obtained through EQE using Equation (1).^[27] The equivalence of J_{sc} calculated using EQE and J_{sc} calculated from J - V measurement is a robust metric to conclude the reliability of measured solar cell efficiency.^[28]

$$J_{sc(\text{EQE})} = \int_{\lambda_1}^{\lambda_2} \frac{q\lambda}{hc} \{EQE(\lambda)AM1.5G(\lambda)\} d\lambda \quad (1)$$

where $J_{sc(\text{EQE})}$ is the short circuit calculated using data obtained for EQE, $EQE(\lambda)$ is the EQE measured for each wavelength between λ_1 and λ_2 , and $AM1.5G(\lambda)$ is the wavelength dependent solar irradiance. The AM1.5G Global spectrum is designed for flat plate modules and has an integrated power of 1000 W m⁻² or 100 mW cm⁻². To understand the surface characteristics and construct the band diagram of the solar cells, X-Ray photoelectron spectroscopy (XPS) and UV photoelectron spectroscopy (UPS) (Thermo ESCALAB250Xi) were employed.

3. Results and Discussion

Results discussed in this article can be broadly divided into four subsections: 1) the effect of bilayer selective contacts, 2) the effect of BSF layer, 3) the effect off-axis substrate, and 4) loss analysis and future potential of the device.

3.1. Effect of Bilayer Selective Contact

To understand the effect of bilayer selective contact, for device 1, we prepare four different samples with four configurations of ESC including only ZnO, only TiO₂, ZnO/TiO₂ bilayer, and TiO₂/ZnO bilayer, and compare their open-circuit voltage. Figure 2 shows the measured V_{oc} for these four configurations of ESC for at least three samples. It is apparent that for both only ZnO and only TiO₂ samples, the V_{oc} is almost similar at around 860–890 mV. This is understandable considering both ZnO and TiO₂ have a similar bandgap, and they show type-II band alignment with i -InGaP/ i -GaAs. They act as ESC because both ZnO and TiO₂ can achieve high n -type conductivity due to oxygen defects and also form a small conduction band offset and large valence band offset with i -InGaP/ i -GaAs, which allows for electron flow but restricts the flow of holes from the i -GaAs absorber layer.^[9,19] We have reported similar results for InP solar cells, where both ZnO and TiO₂ have shown similar performance in terms of V_{oc} .^[9,29] In comparison to single-layer selective contact, a higher V_{oc} can be realized for TiO₂/ZnO bilayer selective contact, and the opposite trend is seen for the ZnO/TiO₂ bilayer (see Figure 2). This difference can be understood in terms of the interface dipole moment, which affects the band alignment and the transport of electrons across the interface by influencing the concentration of charge carriers at the interface. The interface dipole moment can either improve or be detrimental to the overall performance of solar cells depending on the direction of the dipole moment.^[30] Below we briefly discuss the effect of dipole moment at the interface.

In bulk (nonferroelectric), the microscopic dipole moment is vanishingly small because of the randomness in amorphous materials or lattice symmetry in crystalline materials. However, at the interface, the asymmetric distribution of free

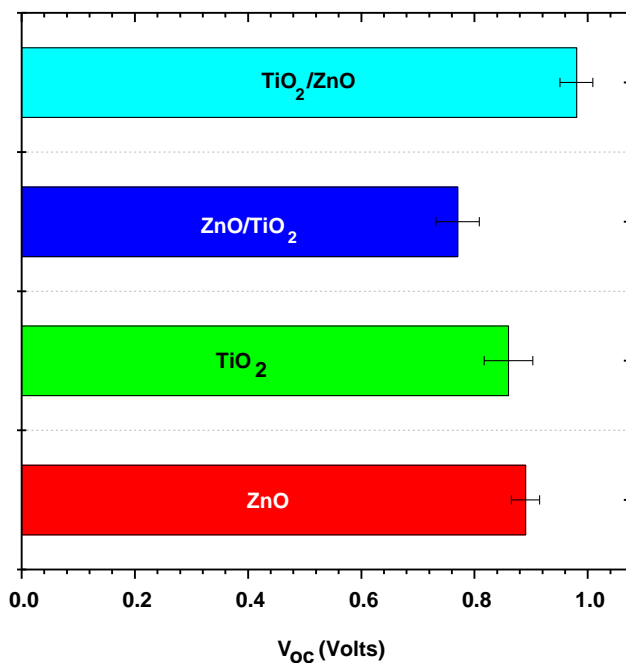


Figure 2. Effect of single- and bilayer ESCs on the V_{oc} of the solar cell.

charges such as ions lead to dipole moment that can be approximated as multiple individual dipole moment aligned in one direction. When there is more than one interface, each interface can lead to a measurable dipole moment, and the overall dipole moment is the vector sum of the dipole moment at the individual interfaces. The effect of dipole moment can be measured in terms of a voltage drop from the positive to negative charge side and is given by the following equation^[31]

$$\delta = \frac{n\vec{p}}{\epsilon_0\epsilon}; \quad \text{where } \vec{p} = q\vec{d} \quad (2)$$

where \vec{p} is the electric dipole moment, and its magnitude is equal to the charge q multiplied by the distance between charges \vec{d} . As per convention, the direction of the dipole moment is from negative to positive charge. Also, n in the above equation denotes the density of the electrical dipole, and ϵ and ϵ_0 , respectively, are the dielectric constant of the material within which the dipole is confined and the dielectric constant of air. The electrostatic nature of

the dipole directly influences the band bending at the interface (by modifying the work function), and influences the transport and density of charges near the interface. Such modification can be illustrated by drawing the band diagram of the solar cell.

Figure 3 shows the band diagram drawn using SCAPS-1D simulation software for three different scenarios: a) solar cell with only ZnO, b) solar cell with ZnO/TiO₂ bilayer, and c) solar cell with TiO₂/ZnO bilayer. It can be seen that in the presence of ZnO/TiO₂ bilayer, the electron quasi-Fermi level bends further downward in comparison to the quasi-Fermi level for only ZnO sample, leading to a lower V_{oc} . This can also be interpreted as a reduction in the available charge carriers near the interface in the presence of ZnO/TiO₂ bilayer near V_{oc} . An opposite effect can be seen for TiO₂/ZnO bilayer, where the dipole positively influences the V_{oc} of the solar cell because the band bending near the interface moves the electron quasi-Fermi level upward compared to that of only ZnO sample. In other words, in comparison to only ZnO, the TiO₂/ZnO bilayer

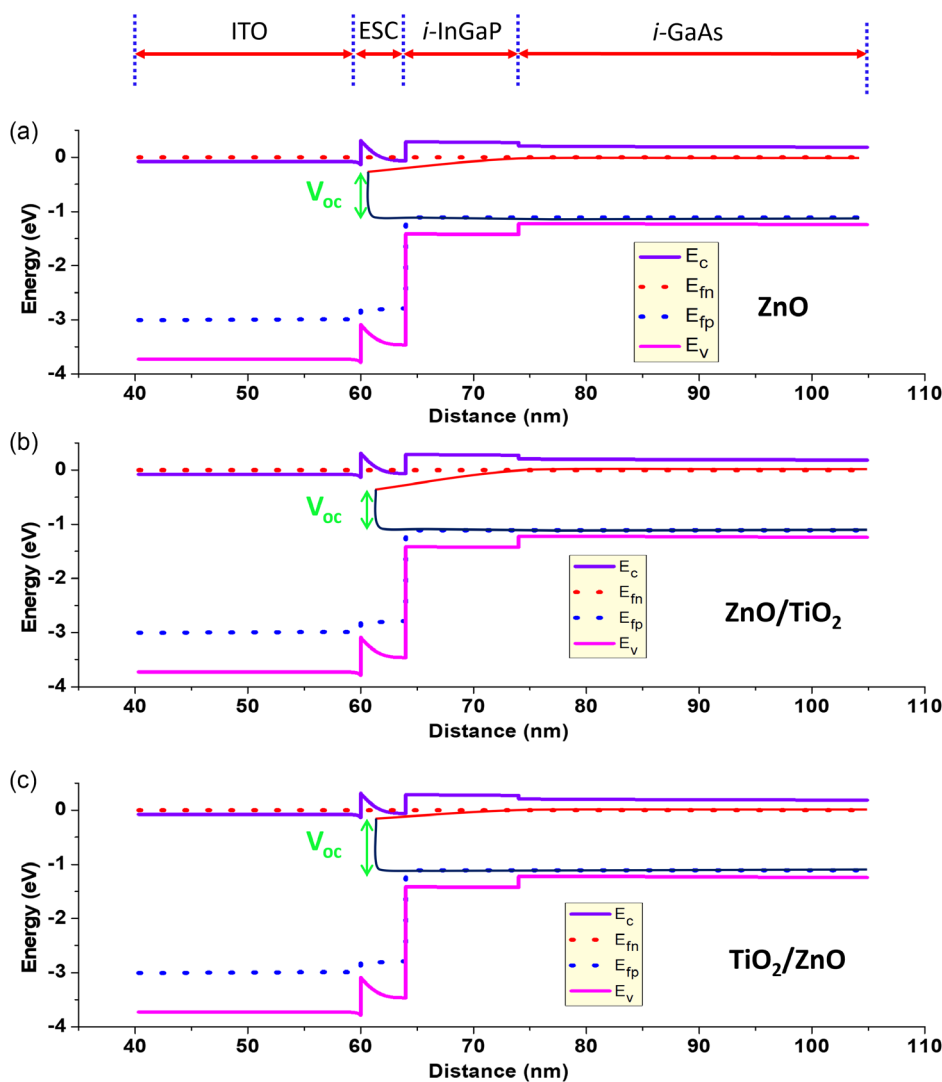


Figure 3. Band diagram for bilayer ESC solar cells: a) band diagram of solar cell with only ZnO as ESC, b) band diagram of solar cell with ZnO/TiO₂ bilayer selective contact, and c) band diagram of solar cell with TiO₂/ZnO bilayer selective contact.

leads to higher electron density near the interface near V_{oc} , and larger electron and hole quasi-Fermi-level splitting, which is reflected in higher V_{oc} .

To understand the origin of dipoles in our solar cells and substantiate our hypothesis, we perform an XPS depth profile analysis. **Figure 4** shows the analysis of Zn $2p_{3/2}$ peak of solar cells with a) only ZnO, b) ZnO/TiO₂ bilayer, and c) TiO₂/ZnO bilayer. Our solar cell structure consists of a complex stack of ITO/ESC/*i*-InGaP/*i*-GaAs/*p*⁺⁺-InGaP/*p*⁺-GaAs, and the ESC that we study using depth profile XPS is: ZnO, ZnO/TiO₂, and TiO₂/ZnO. This significantly restricts our ability to draw an accurate band diagram using the data obtained from depth profile XPS and UPS. Therefore, we restrict ourselves to studying the shift in cation core level, which can provide very useful information regarding the chemical and physical environment of the compound, and dipole moment at the interface. Moreover, for simplicity, we only study Zn $2p_{3/2}$ core level as we are comparing the bilayer selective contact with ZnO. Figure 4a shows the core level spectra from Zn $2p_{3/2}$ at different depths for only ZnO sample for device 1. Zn $2p_{3/2}$ peak near the ITO/ZnO interface has a binding of 1022.2 eV showing a positive shift in the binding energy (BE) compared to bulk ZnO (BE = 1022.0 eV), and the dipole moment is aligned in the ITO→ZnO direction. However, with increasing

depth, Zn $2p_{3/2}$ shows a BE of 1022.0 eV, which corresponds to bulk ZnO, and with further increase in depth profiling, Zn $2p_{3/2}$ shifts negatively to 1021.7 eV, which shows that the dipole near the ZnO/*i*-InGaP interface is aligned from ZnO→*i*-InGaP. On the contrary, in the case of ZnO/TiO₂ bilayer sample, the shift in the Zn $2p_{3/2}$ BE near ITO/ZnO interface is significantly positively shifted to 1022.5 eV, which shows the addition of ZnO on top of TiO₂ leads to additional dipole moment in the direction opposite to the direction of built-in electric field. Further increase in the depth returns the shift in Zn $2p_{3/2}$ core level back to 1022.2 eV, but is still 0.2 eV higher than the bulk ZnO core level, signifying that even near the ZnO/*i*-InGaP interface, the dipole remains aligned opposite to the direction of the built-in electric field, leading to a lower V_{oc} . On the other hand, a completely opposite trend can be seen for TiO₂/ZnO samples, where the shift in Zn $2p_{3/2}$ core level is minimal even near the TiO₂/ZnO interface, and the core BE remains fixed at 1022.0 eV. Moreover, with increased depth profile time, there is no shift in the core BE, which may signify that the dipole at ITO/TiO₂/ZnO interface compensates for the dipole at the ZnO/*i*-InGaP interface, leading to the highest efficiency in case of TiO₂/ZnO bilayer sample. Note that the dipoles at the interface influence the band bending causing interfacial charge transfer and modified charge

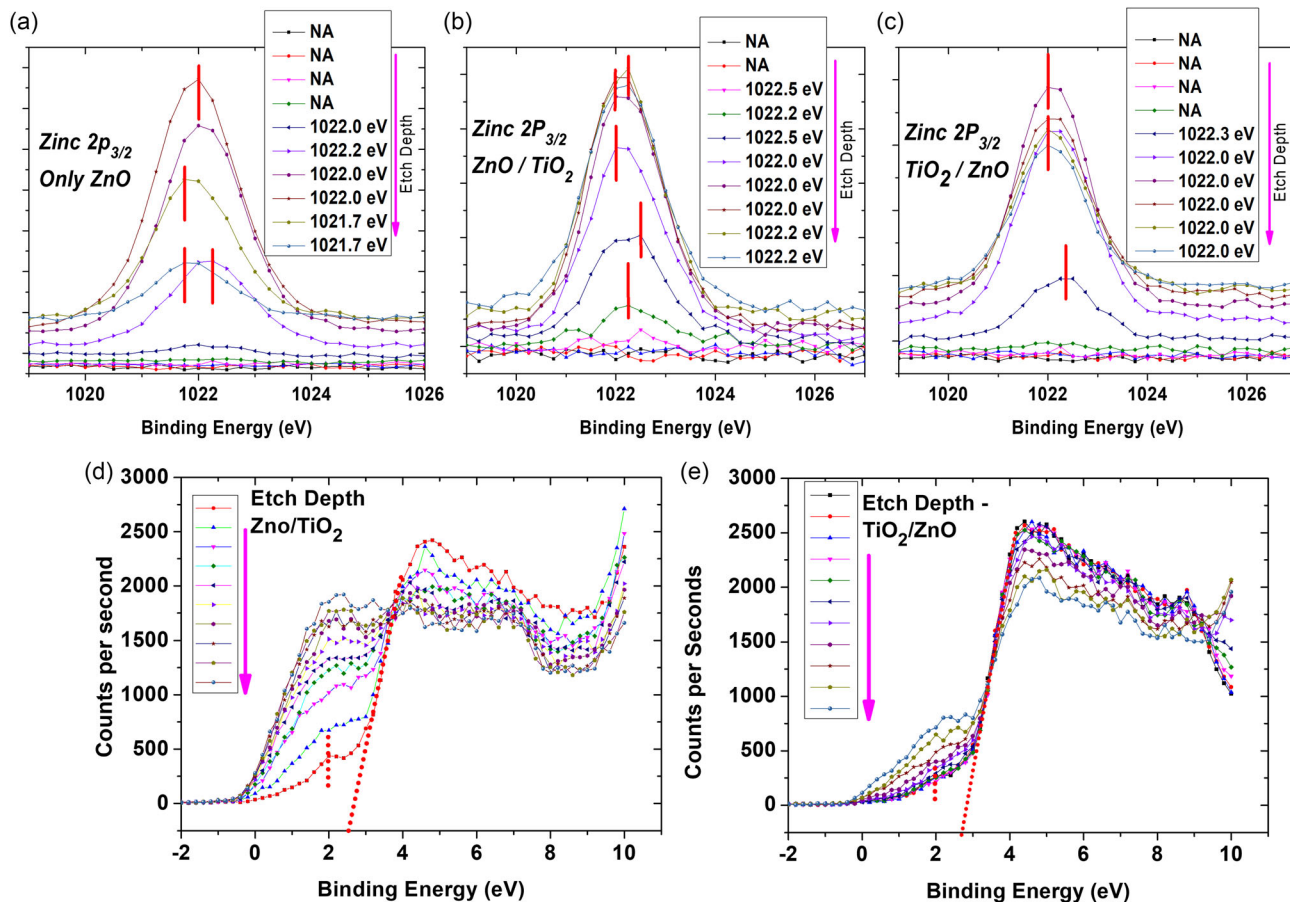


Figure 4. XPS depth profile of Zn $2p_{3/2}$ core level and valence band for different types of solar cells compared in this article: a) Zn $2p_{3/2}$ core level for solar cell with only ZnO as ESC, b) Zn $2p_{3/2}$ core level for ZnO/TiO₂ bilayer ESC solar cell, and c) Zn $2p_{3/2}$ core level for TiO₂/ZnO bilayer solar cell. d) Depth profile of valence band of ZnO/TiO₂ bilayer solar cell and e) depth profile of valence band of TiO₂/ZnO solar cell.

carrier density at the interface. Therefore, next, we perform XPS depth profile of the valence band of ZnO/TiO₂ and TiO₂/ZnO samples.

Figure 4d,e, respectively, show the depth profile of the valence band of ZnO/TiO₂ and TiO₂/ZnO samples. In the case of ZnO/TiO₂, we see an accumulation of holes near the interface with increasing depth (Figure 4d), as evidenced by the increasing density of occupied states in the valence band (between 0 and 3 eV), whereas a depletion of holes and accumulation of electrons at the interface of ESC would be more beneficial. In contrast, we do not see an accumulation of holes near the interface in the case TiO₂/ZnO samples, which may be a result of compensated dipole moment at the ZnO/*i*-InGaP interface. Overall, it can be postulated that in the case of TiO₂/ZnO samples, the electron density at the interface is significantly enhanced, whereas in the case of ZnO/TiO₂ case, the electron density at the interface is significantly reduced due to the accumulation of holes at the ZnO/*i*-InGaP interface, which is expected from the band diagram shown in Figure 3.

3.2. Effect of BSF

The benefits of BSF have been known to the solar cell community for a long time.^[24] BSF creates a built-in electric field in the direction same as the built-in electric field due to the p-n junction, thereby aiding the V_{oc} of the solar cell. Moreover, as early as

1977,^[25] it was clear that in addition to the built-in electric field, BSF also ensures decreased diffusivity and reduced conductivity of electrons (minority carriers) near the back contact, which substantially contributes to the enhancement in the V_{oc} of the solar cell. In other words, BSF can be understood as a highly efficient barrier for electron flow (or as hole-selective contact). A more detailed discussion on the topic can be found in refs. [12,19]. Here, we are investigating how much effect BSF can have on V_{oc} in the presence of a bilayer selective contact. **Figure 5a** shows the current density versus voltage (J - V) for solar cells with and without BSF for on-axis samples. It is evident that in the presence of a BSF layer, a higher V_{oc} can be obtained for solar cells with optimized bilayer selective contact. The V_{oc} without the BSF layer was 0.96 V, whereas the V_{oc} in the presence of the BSF layer was 0.98 V, confirming that BSF can indeed improve the V_{oc} of solar cells. However, there was a slight decrease in the J_{sc} of the solar cell in the presence of the BSF layer, as evidenced by the wavelength-dependent J_{sc} measurement of solar cells with and without BSF shown in Figure 5b. It can be seen that for wavelengths below 580 nm, there is a slight decrease in J_{sc} in the presence of BSF, which overcompensates for any improvement in the J_{sc} above 580 nm due to improved charge collection near the back contact in the presence of BSF layer. We believe the decrease in J_{sc} as a function of wavelength below 580 nm may be due to the poor epitaxial quality of the front *i*-InGaP passivation layer, in the case of a BSF containing solar cell. However, a more extensive study is required to conclusively

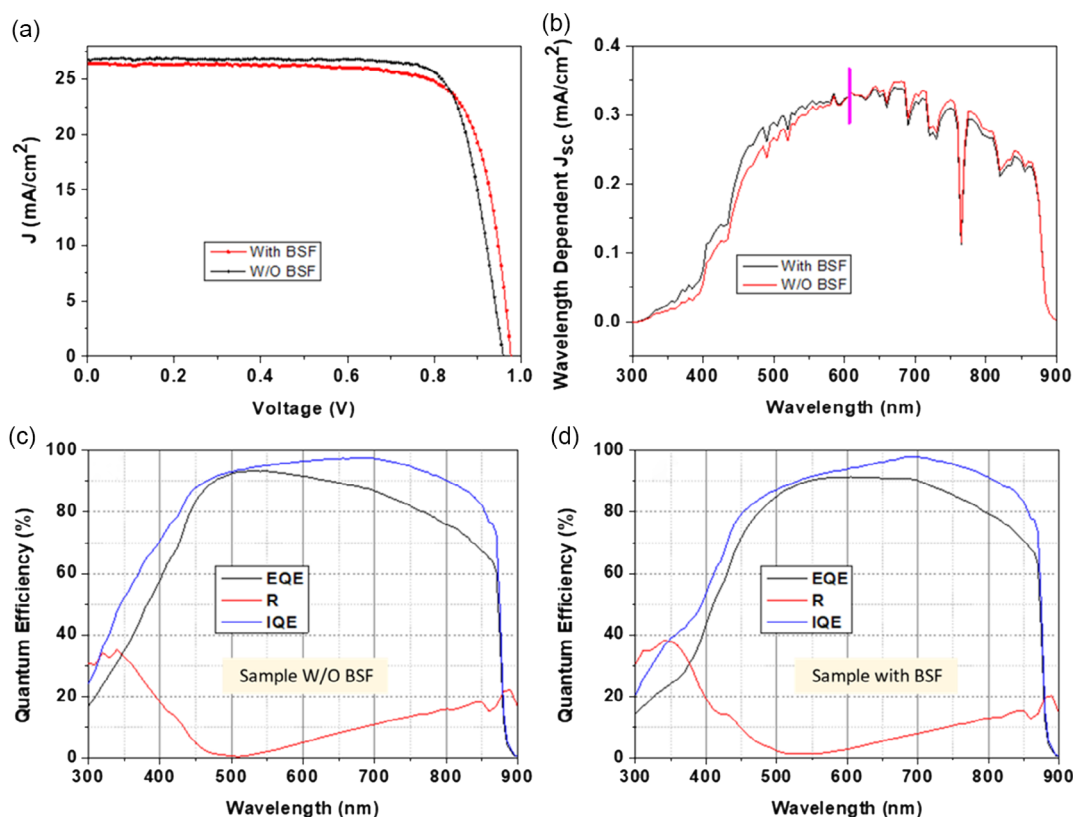


Figure 5. a) Comparative J - V characteristics of solar cells grown on on-axis substrate (device 1), with and without BSF layer; b) comparative J_{sc} versus wavelength graph of solar cell with and without BSF for on-axis samples (device 1); and c,d) shows the EQE, R, and IQE of on-axis solar cell samples, with and without BSF.

pinpoint the origin of this loss in the presence of a heavily doped BSF layer. Moreover, the doping and thickness of the BSF layer can be optimized to improve the performance of the device. Figure 5c,d shows the corresponding overlaid EQE, reflectance (R), and internal quantum efficiency (IQE) versus wavelength graphs for the bilayer devices with and without BSF layer.

3.3. Effect of 6° Off-Axis Substrates

It is well known that the growth of InGaP on 6° off-axis substrate can improve the quality of the epilayer by improving the overall ordering of cations during epilayer growth.^[21] Therefore, to further improve the performance of our devices, we grow BSF layer, and i -GaAs absorber layer along with i -InGaP passivation on 6° off-axis substrates followed by deposition of optimized bilayer selective contact. In agreement with previous results, we find that the overall performance of our solar cell is significantly improved mainly because of the improved V_{oc} . **Figure 6a** shows the comparative J - V characteristics of solar cells fabricated for off-axis and on-axis substrates. The off-axis device can reach a V_{oc} of

1.04 V and in comparison, the maximum V_{oc} obtained for the on-axis device is only 0.98 V. Also, the results are highly reproducible, at least across three different samples, giving an average V_{oc} of 1.02 ± 0.02 V for devices grown on off-axis substrates. The maximum efficiency obtained for the off-axis substrate was 21.2% with a V_{oc} of 1.04 V, J_{sc} of 26.2 mA cm^{-2} , and a fill factor of 77.8%. Figure 6b shows the J - V characteristic corresponding to the best device. Overall, we find that the use of bilayer selective contact on epilayers grown on the off-axis substrate is optimum for achieving high-efficiency solar cells.

3.4. Current Loss Analysis at MPP

To better understand the origin of losses and the future potential of our solar cells, we perform a current loss analysis based on the method proposed by Armin et al. The current loss analysis takes into account several different loss mechanisms including total resistance loss due to both high series and low shunt resistance, total optical loss due to metal shading and imperfect antireflective coating, and total recombination loss. Two of the biggest

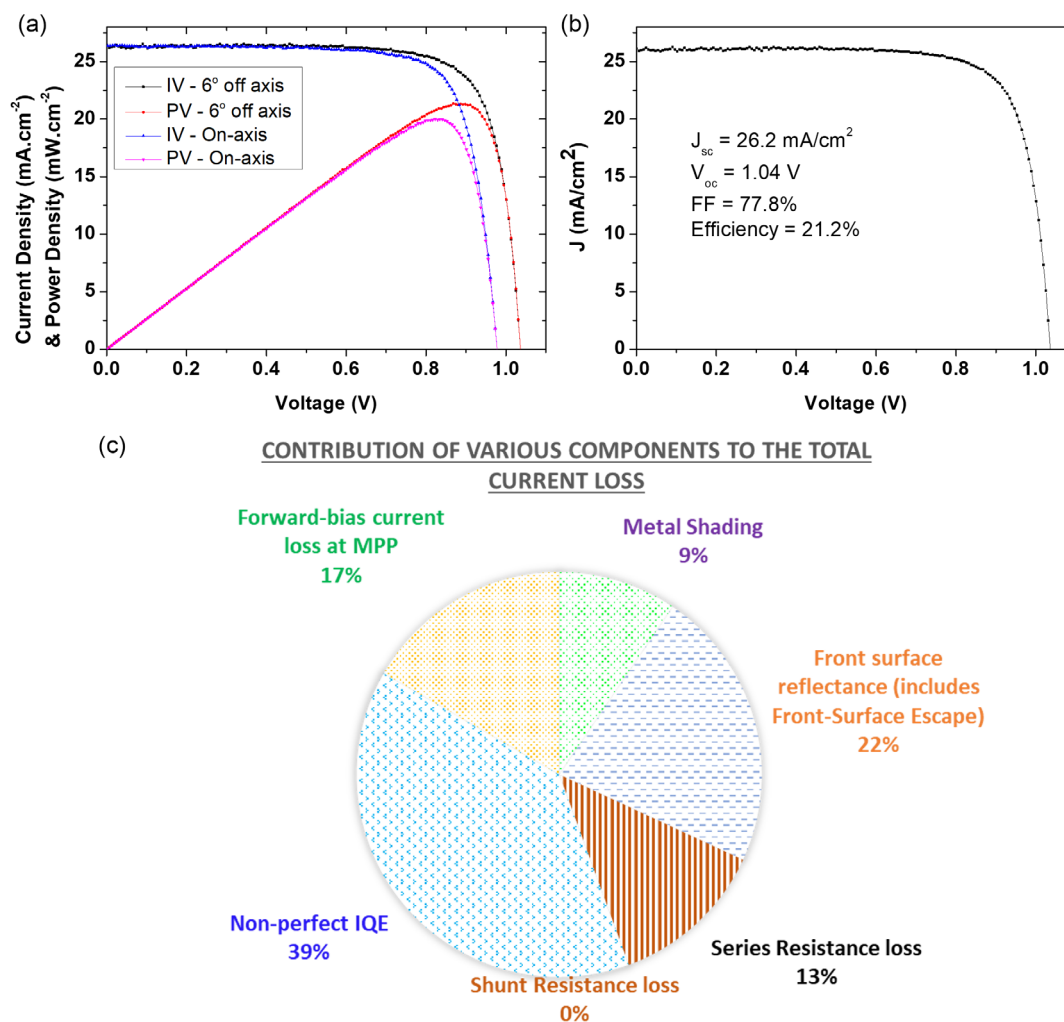


Figure 6. a) Comparative J - V characteristics for solar cells grown on on-axis and off-axis substrates with BSF layer. b) J - V characteristic for the best off-axis solar cell. c) Percentage contribution of different loss mechanisms to the total power loss at the maximum power point.

losses accounting for about 80% of the total loss come from recombination and front surface reflectance loss. In particular, recombination loss accounts for more than 5.5 mA cm^{-2} of current density at maximum power point. To get better insight into recombination, we can further analyze the IQE spectra shown in Figure 5d. First, the quality of our *i*-GaAs layer is relatively inferior with a minority carrier lifetime of 240 ps and the recombination in the bulk is one of the primary contributions to the current loss due to recombination. Moreover, at lower wavelengths (350–500 nm), only about 80% IQE can be achieved (see Figure 5d) for the BSF device, which, as we hypothesized earlier, is because of the nonoptimal thickness and quality of the InGaP layer, used for passivation and BSF, which can be further improved by improving the growth parameters. Also, note that even without BSF (see Figure 5c), the maximum IQE achieved is only 90% at a shorter wavelength, showing that there is some loss in both the *i*-GaAs and the front passivation/charge collection layer. For both BSF and non-BSF samples, the loss in IQE is almost similar at longer wavelengths (700–870 nm), which points to a common origin of loss. We postulate that IQE loss at longer wavelengths is because of the low quality of *i*-GaAs layer, and the parasitic absorption/collection losses in p^+ -GaAs substrate. However, a more thorough investigation is required to confirm the origin of this loss. In terms of optical losses, most of the loss is from a nonoptimal antireflective coating. A trilayer antireflective coating consisting of MgF_2 may be used to achieve an antireflectance across a broadband solar spectrum. Finally, the series resistance of the solar cell accounts for about 13% of the total power loss, which can be improved by decreasing the sheet resistance of ITO and by using a thicker metal front contact.

4. Conclusion

In conclusion, we showed that in comparison to a single-layer ESC, a bilayer selective contact is more efficient, as it modifies the interface electrostatics, and improves the charge carrier collection and transport. Using an optimized selective contact of TiO_2/ZnO bilayer, we achieve a V_{oc} as high as 0.96 V. We have performed an in-depth XPS analysis to further elucidate the origin of interface modification in presence of a bilayer selective contact. We also showed that a further improvement in V_{oc} can be achieved if the optimized bilayer selective contact is applied in conjunction with a BSF grown on 6° off-axis substrate. Our best device showed a V_{oc} of 1.04 V, which is very near to the highest reported V_{oc} for substrate-based p - n junction GaAs solar cells. Furthermore, we also perform an in-depth analysis to better understand the losses in our solar cells and to strategize the steps for future improvement of these solar cells. Results reported in this article are important for a new generation of GaAs solar cells based on charge carrier selective contacts.

Acknowledgements

Australian Research Council and Australian Renewable Energy Research Agency are acknowledged for financial support. Access to the epitaxial growth and device fabrication facilities is provided through the Australian National Fabrication Facility, ACT node. Drs B. Gong and

S.Y. Yin from the Surface Analysis Laboratory of UNSW are acknowledged for support with depth profile XPS of the devices.

Conflict of Interest

The authors declare no conflict of interest.

Author Contributions

V.R. and T.H. contributed equally. V.R. fabricated and characterized the devices, and T.H. performed the MOCVD growth and growth-related characterization. H.H.T. and C.J. supervised the project. V.R. conceptualized the project and wrote the manuscript with contributions from all the authors. All authors have given approval to the final version of the manuscript.

Data Availability Statement

The data that support the findings of this study are available from the corresponding author upon reasonable request.

Keywords

III-V, carrier selective contact, gallium arsenide, photovoltaics, XPS/UPS

Received: November 1, 2023

Revised: December 27, 2023

Published online: February 2, 2024

- [1] V. Raj, T. Haggren, W. W. Wong, H. H. Tan, C. Jagadish, *J. Phys. D: Appl. Phys.* **2022**, *55*, 143002.
- [2] a) J. Li, A. Aierken, Y. Liu, Y. Zhuang, X. Yang, J. H. Mo, R. K. Fan, Q. Y. Chen, S. Y. Zhang, Y. M. Huang, Q. Zhang, *Front. Phys.* **2021**, *8*, 631925; b) R. Verduci, V. Romano, G. Brunetti, N. Yaghoobi Nia, A. Di Carlo, G. D'Angelo, C. Ciminelli, *Adv. Energy Mater.* **2022**, *12*, 2200125.
- [3] K. A. Horowitz, T. W. Remo, B. Smith, A. J. Ptak, *A Techno-Economic Analysis and Cost Reduction Roadmap for III-V Solar Cells*, National Renewable Energy Lab.(NREL), Golden, CO, United States **2018**.
- [4] a) J. S. Ward, T. Remo, K. Horowitz, M. Woodhouse, B. Sopor, K. VanSant, P. Basore, *Progr. Photovoltaics* **2016**, *24*, 1284; b) O. M. Saif, A. H. Zekry, M. Abouelatta, A. Shaker, *Silicon* **2023**, *15*, 6329; c) M. A. Fazal, S. Rubaiee, *Solar Energy* **2023**, *258*, 203.
- [5] A. K.-W. Chee, *Renewable Sustainable Energy Rev.* **2023**, *173*, 113027.
- [6] a) R. Kapadia, Z. Yu, H.-H. H. Wang, M. Zheng, C. Battaglia, M. Hettick, D. Kiriya, K. Takei, P. Lobaccaro, J. W. Beeman, J. W. Ager, R. Maboudian, D. C. Chrzan, A. Javey, *Sci. Rep.* **2013**, *3*, 2275; b) M. Zheng, K. Horowitz, M. Woodhouse, C. Battaglia, R. Kapadia, A. Javey, *Progr. Photovoltaics* **2016**, *24*, 871; c) M. Yao, J. B. Rawlings, T. F. Kuech, *Semicond. Sci. Technol.* **2020**, *35*, 105011; d) Y. Shoji, R. Oshima, K. Makita, A. Ubukata, T. Sugaya, *IEEE J. Photovoltaics* **2021**, *11*, 93.
- [7] a) V. Raj, F. Rougieux, L. Fu, H. H. Tan, C. Jagadish, *IEEE J. Photovoltaics* **2020**, *10*, 1657; b) V. Raj, H. H. Tan, C. Jagadish, *Asian J. Phys.* **2020**, *28*, 719; c) V. Raj, K. Vora, L. Fu, H. H. Tan, C. Jagadish, *ACS Nano* **2019**, *13*, 12015.
- [8] V. Raj, D. Chugh, L. E. Black, M. M. Shehata, L. Li, F. Kremer, D. H. Macdonald, H. H. Tan, C. Jagadish, *npj 2D Mater. Appl.* **2021**, *5*, 12.

- [9] V. Raj, T. S. dos Santos, F. Rougieux, K. Vora, M. Lysevych, L. Fu, S. Mokkaleti, H. H. Tan, C. Jagadish, *J. Phys. D: Appl. Phys.* **2018**, *51*, 395301.
- [10] V. Raj, L. Fu, H. H. Tan, C. Jagadish, *IEEE J. Photovoltaics* **2019**, *9*, 980.
- [11] V. Raj, H. H. Tan, C. Jagadish, *Appl. Mater. Today* **2020**, *18*, 100503.
- [12] U. Würfel, A. Cuevas, P. Würfel, *IEEE J. Photovoltaics* **2015**, *5*, 461.
- [13] a) M. Taguchi, *ECS J. Solid State Sci. Technol.* **2021**, *10*, 025002; b) H. Lin, M. Yang, X. Ru, G. Wang, S. Yin, F. Peng, C. Hong, M. Qu, J. Lu, L. Fang, C. Han, P. Procel, O. Isabella, P. Gao, Z. Li, X. Xu, *Nat. Energy* **2023**, *8*, 789.
- [14] F. H. Isikgor, S. Zhumagali, L. V. T. Merino, M. De Bastiani, I. McCulloch, S. De Wolf, *Nat. Rev. Mater.* **2023**, *8*, 89.
- [15] a) B. Roose, Q. Wang, A. Abate, *Adv. Energy Mater.* **2019**, *9*, 1803140; b) T. Baumeler, A. A. Saleh, T. A. Wani, S. Huang, X. Jia, X. Bai, M. Abdi-Jalebi, N. Arora, M. Grätzel, M. I. Dar, *ACS Mater. Lett.* **2023**, *5*, 2408.
- [16] T. Amrillah, A. Prasetio, A. R. Supandi, D. H. Sidiq, F. S. Putra, M. A. Nugroho, Z. Salsabilla, R. Azmi, *Mater. Horiz.* **2023**, *10*, 313.
- [17] a) V. Raj, K. Vora, L. Li, L. Fu, H. H. Tan, C. Jagadish, presented at 2019 *Compound Semiconductor Week (CSW)*, Nara, Japan, May **2019**; b) V. Raj, T. Lu, M. Lockrey, R. Liu, F. Kremer, L. Li, Y. Liu, H. H. Tan, C. Jagadish, *ACS Appl. Mater. Interfaces* **2019**, *11*, 24254.
- [18] a) J. Li, T. Pan, J. Wang, S. Cao, Y. Lin, B. Hoex, Z. Ma, L. Lu, L. Yang, B. Sun, D. Li, *ACS Appl. Mater. Interfaces* **2020**, *12*, 36778; b) D. Wang, N. K. Elumalai, M. A. Mahmud, M. Wright, M. B. Upama, K. H. Chan, C. Xu, F. Haque, G. Conibeer, A. Uddin, *Org. Electron.* **2018**, *53*, 66; c) C. M. Pelicano, H. Yanagi, *J. Energy Chem.* **2018**, *27*, 455.
- [19] V. Raj, T. Haggren, J. Tournet, H. H. Tan, C. Jagadish, *ACS Appl. Energy Mater.* **2021**, *4*, 1356.
- [20] T. Haggren, V. Raj, A. Haggren, N. Gagrani, C. Jagadish, H. Tan, *ACS Appl. Mater. Interfaces* **2022**, *14*, 52918.
- [21] a) A. Gomyo, S. Kawata, T. Suzuki, S. Iijima, I. Hino, *Jpn. J. Appl. Phys.* **1989**, *28*, L1728; b) A. S. Brown, U. K. Mishra, J. A. Henige, M. J. Delaney, *J. Appl. Phys.* **1988**, *64*, 3476.
- [22] Z. Li, Y. Zeng, Y. Song, J. Zhang, Y. Zhou, Y. Ning, L. Qin, L. Wang, *Appl. Sci.* **2021**, *11*, 8639.
- [23] a) R. S. Goldman, K. L. Kavanagh, H. H. Wieder, S. N. Ehrlich, R. M. Feenstra, *J. Appl. Phys.* **1998**, *83*, 5137; b) N. H. Rafat, S. M. Bedair, P. R. Sharps, J. S. Hills, J. A. Hancock, M. L. Timmons, presented at *Proc. of 1994 IEEE 1st World Conf. on Photovoltaic Energy Conversion – WCPEC (A Joint Conf. of PVSC, PVSEC and PSEC)*, Waikoloa, HI, USA, December **1994**; c) A. van Geelen, P. R. Hageman, G. J. Bauhuis, P. C. van Rijsingen, P. Schmidt, L. J. Giling, *Mater. Sci. Eng.: B* **1997**, *45*, 162.
- [24] P. D. Demoulin, M. S. Lundstrom, R. J. Schwartz, *Solar Cells* **1987**, *20*, 229.
- [25] J. G. Fossum, *IEEE Trans. Electron Devices* **1977**, *24*, 322.
- [26] A. Cuevas, D. Yan, *IEEE J. Photovoltaics* **2013**, *3*, 916.
- [27] <https://nanohub.org/resources/jscfromeqe> (accessed: September 2023).
- [28] a) H. J. Snaith, *Nat. Photonics* **2012**, *6*, 337; b) *Nat. Mater.* **2015**, *14*, 1073.
- [29] B. Gupta, M. M. Shehata, Y. Lee, L. E. Black, F. Ma, B. Hoex, C. Jagadish, H. H. Tan, S. Karuturi, *Solar RRL* **2023**, *7*, 2200868.
- [30] a) D. Cahen, A. Kahn, *Adv. Mater.* **2003**, *15*, 271; b) H. Ishii, K. Sugiyama, E. Ito, K. Seki, *Adv. Mater.* **1999**, *11*, 605; c) G. Ashkenasy, D. Cahen, R. Cohen, A. Shanzer, A. Vilan, *Acc. Chem. Res.* **2002**, *35*, 121.
- [31] H. J. Lee, A. C. Jamison, T. R. Lee, *Acc. Chem. Res.* **2015**, *48*, 3007.